inorganics

MDPI

Article

ZrO_2 Coating for Surface Functionalization of Jianshui Purple Pottery: A Sol-Gel Approach with Antibacterial Performance

Zhenwei Gan [1], Jinlin He [2,3], Jing Liu [1,2], Peng Zhang [1,2,*], Aidang Shan [1,2], Qinxiao Na [2,3], Yu He [4], Yuan Bao [4], Zixuan He [4] and Lian Gao [1,2]

[1] School of Materials Science and Engineering, Shanghai Jiao Tong University, Shanghai 200240, China
[2] Shanghai Jiao Tong University-Jianshui Purple Pottery Joint Research Center, Honghe 654300, China
[3] Shanghai Jiao Tong University Yunnan (Dali) Research Institute, Dali 671000, China
[4] Jianshui Chongwen Tongchuang Purple Clay Culture Co., Ltd., Honghe 654300, China
* Correspondence: pengzhang2010@sjtu.edu.cn; Tel.: +86-136-5185-0686

Abstract

The surface decoration techniques, such as incising-filling, glaze spraying, wood firing, and secondary low-temperature refiring, etc., have been widely used for traditional potteries, such as Jianshui purple pottery. These surface modifications are mainly for artistic expression, whereas functional surface modification has barely been reported. The development of novel coating materials and processes is an alternative path for the innovation of traditional pottery. However, the surface functional materials often peel or detach from the pottery body after high-temperature sintering. It is thus imperative to develop coating materials and processes with robust adhesion and accommodation for secondary functional materials. Through the screening of different $ZrO(OH)_2$ sols and coating processes, the coating of $ZrO(OH)_2$ sol on the 800 °C baked Jianshui purple pottery achieved uniform and tight surface coating. Reducing the colloidal particle size and particle concentration in the sol, as well as Y^{3+} doping, is also conductive to the structural stability of the coatings. Additional loading of silver nanoparticles onto the ZrO_2 coating layer effectively endows the pottery with antibacterial performance. The coated samples loaded with silver nanoparticles exhibited an antibacterial rate of 32.7% after accelerated desorption, demonstrating potential for functional pottery applications.

Keywords: Jianshui purple pottery; surface modification; coating; ZrO_2; antibacterial

1. Introduction

Jianshui purple pottery is a traditional ceramic, renowned for its surface decoration techniques of "incising and filling" and "unglazed polishing." Additionally, products featuring natural ash glaze formed through wood firing, known as "naked firing," are also popular, as the surface texture, color, and coverage area of the ash glaze are randomly generated, whereas these surface treatments are primarily decorative. With the increasing demand for novel ceramic products in modern life, the requirement for ceramic functionality has become more and more prominent. Relative to porcelain, on which the coating of self-cleaning nanomaterials has been widely used in high-end fixtures, research and products concerning functional surface modifications on pottery are still scarce. This is mainly ascribed to the challenge in the effective adhesion of surface coatings to pottery surfaces. Typically, surface functional coating materials tend to peel or detach from the body after high-temperature sintering due to the heterogenous properties of the coating

Check for updates

Academic Editor: Claudio Pettinari

Received: 31 December 2025
Revised: 3 February 2026
Accepted: 5 February 2026
Published: 9 February 2026

Copyright: © 2026 by the authors. Licensee MDPI, Basel, Switzerland. This article is an open access article distributed under the terms and conditions of the Creative Commons Attribution (CC BY) license.

materials and the pottery [1]. Therefore, the development of novel coating materials and processes to improve the functional properties of purple pottery surfaces represents a new pathway for innovating traditional purple potteries, as well as the other types of pottery.

Applying surface coatings can significantly alter the physical and chemical properties of ceramic surfaces, including surface texture, material strength, colors, and/or functionalities. With the advancement of technologies, surface modifications for ceramics have become diversified and efficient. The primary methods for ceramic surface modification include: (1) physical modification, such as additive manufacturing (AM) to enhance the wear resistance, corrosion resistance, and heat resistance of ceramic surfaces [2]; (2) vapor deposition, including chemical vapor deposition (CVD) [3] and physical vapor deposition (PVD) [4]; (3) ion beam sputtering deposition; (4) plasma treatment [5]; and (5) surface coating [6], as demonstrated by Zhang et al. [7], who employed a heterogeneous nucleation method through surface chemical coating to achieve functional modification of ceramic powders.

The aforementioned methods for ceramic surface modification, additive manufacturing, ion beam sputtering deposition, and plasma treatment are difficult to apply on pottery products due to the cost and complexity of production. Surface coating is thus applied for the surface modification of purple pottery. General methods for surface coating include thermal spraying [8], cold spraying [9], and the sol–gel method [10], among which, the sol–gel method is operationally simple and suitable for purple potteries.

In recent years, the sol–gel method has made significant progress in ceramic surface coating, particularly in multifunctional coating design, structural optimization, and performance enhancement. For example, Meng [11] developed a sol system combining nano-boehmite and micro-sized titanium diboride (TiB_2) for multifunctional coatings. Liu et al. [12] claimed that the sol–gel method, through compositional gradient design and nano/micro composite systems (such as Al_2O_3-SiO_2 mixed coatings), can effectively bridge matrix microcracks, improve the flexural strength, and reduce strength dispersion, outperforming single-coating systems. The sol–gel method has become highly mature, allowing for the structural and compositional adjustment of the coating materials through control over the reaction system and various sintering parameters.

This work addresses the gap in functional surface modifications for traditional pottery, aiming to develop a reproducible sol–gel coating process for Jianshui purple pottery.

2. Results

2.1. Particle Sizes of the Sols

The dynamic light scattering (DLS) test results for the four sols are shown in Figure 1. The median sizes of the particles of LSZ, YSZ, HBZ, and LBZ sols are ~50 nm, 60 nm, 90 nm, and 110 nm, respectively. Besides the high-density sample, HBZ, which has a wide size distribution from 25 to 250 nm, the other samples show a relatively narrower size distribution. LSZ, YSZ, and LBZ have sizes of 50 $\pm$ 5 nm, 60 $\pm$ 8 nm, and 110 $\pm$ 30 nm.

2.2. Morphologies of the Surface Coatings

Figure 2 shows the photographs of the 12 samples after applying four different sols (LSZ, LBZ, HBZ, and YSZ) onto three different Jianshui purple pottery bodies (green body, pre-sintered body, and baked body), followed by sintering at 1150 °C. The green, pre-sintered, and baked bodies represent the pottery bodies oven dried at ~60 °C, sintered at 1150 °C, and baked at ~800 °C, respectively. Preliminary macroscopic observation shows that the samples from the same type of body, while coated with different sols, have a similar appearance. In contrast, the appearance of the samples with the same sol precursor applied on different bodies are significantly different.

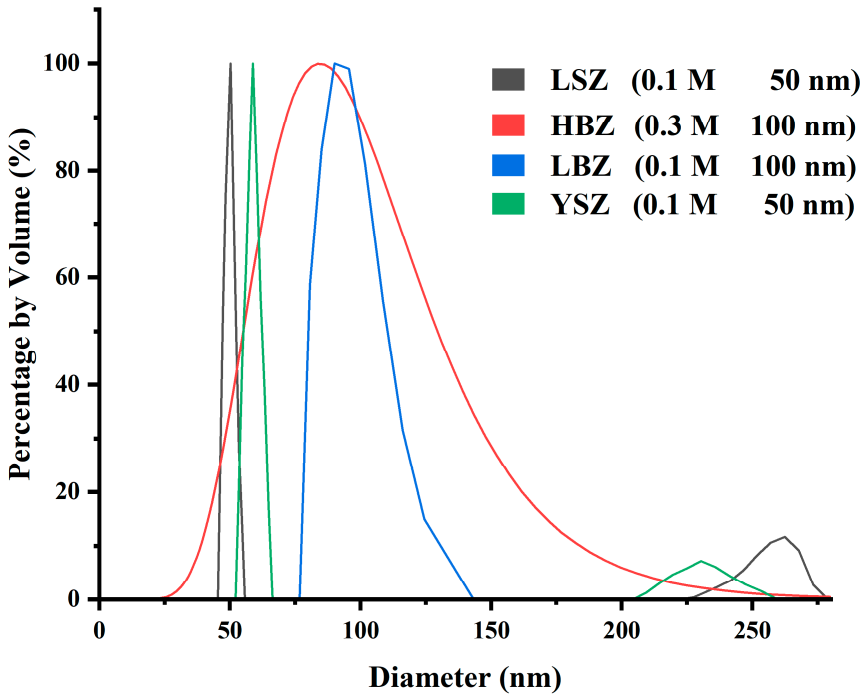


Figure 1. Volumetric distribution diagrams for the four sols: LSZ (low-concentration small-particle size): $D_{average}$(diameter) = 50 nm; LBZ (low-concentration large-particle size): $D_{average}$ = 100 nm; HBZ (high-concentration large-particle size): $D_{average}$ = 90 nm; and YSZ (low-concentration YSZ small-particle): $D_{average}$ = 60 nm.

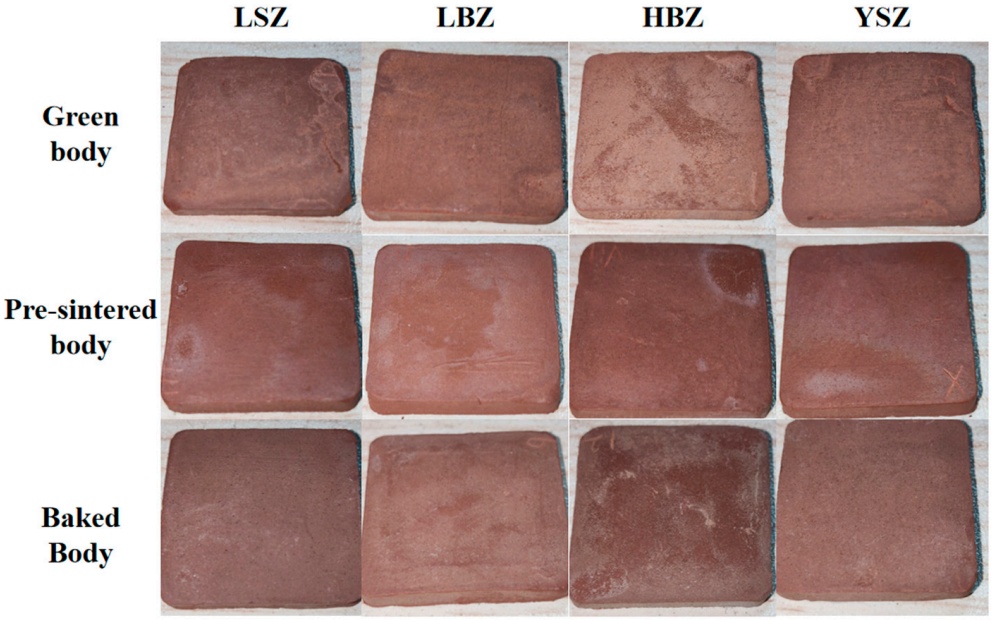


Figure 2. The samples coated with four sols (LSZ, LBZ, HBZ, and YSZ) on green (oven dried at 60 °C) bodies, pre-sintered (1150 °C) bodies, and baked (800 °C) bodies, followed by typical firing process.

The sintered samples with sol coated on the green body exhibited poor surface uniformity. The surface coating was prone to peeling upon scraping, and the detached powders contained red powders from the pottery body. The samples with sol coated on the pre-sintered bodies also showed poor surface uniformity. The coating layer on most of the surface was very thin and adhered strongly to the body. When the samples were achieved with the sol coated on baked (800 °C) pottery bodies, the sintered samples displayed uni-

form surface coatings with strong adhesion to the body underneath. The surface coating layer is difficult to scrape off.

The microstructures of the surfaces from various samples were analyzed by SEM (Figures 3–5).

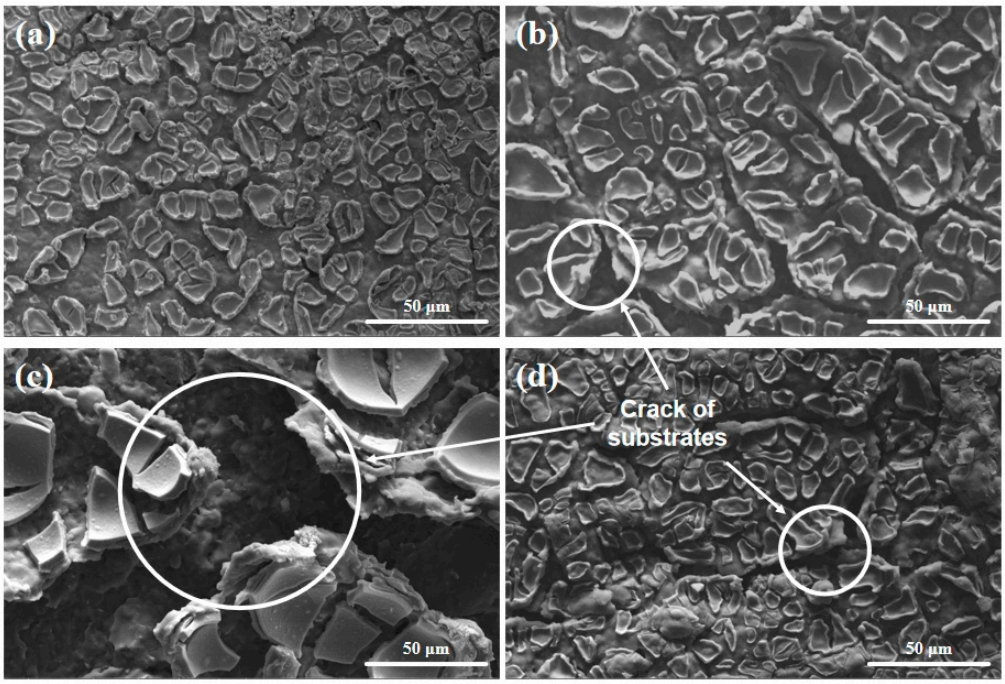


Figure 3. SEM of the samples dip-coated in four different sols: (**a**) LSZ; (**b**) LBZ; (**c**) HBZ; and (**d**) YSZ on the green bodies followed by sintering (1150 °C).

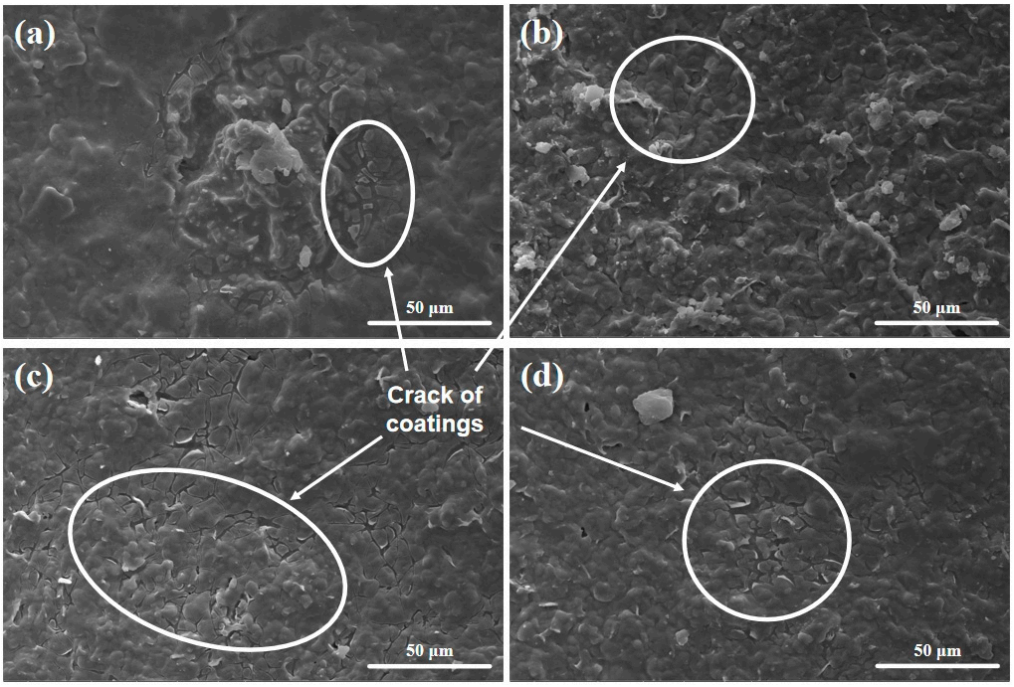


Figure 4. SEM morphologies of the samples dip-coated in four different sols: (**a**) LSZ; (**b**) LBZ; (**c**) HBZ; and (**d**) YSZ on the sintered (1150 °C) bodies, followed by second sintering (1150 °C).

Coated green body samples (Figure 3) show curled broken chips of zirconia with sizes larger than 20 μm on the surface of the body. Most samples also show cracking on the underlying body, except the LSZ sample. This suggests a relatively better distribution of

the zirconia layer on the surface of the body after sintering when the particle concentration of the sol precursor is low.

On the samples with the sols dip-coated on the surface of the pre-sintered body and refired again, the zirconia coating shows a thin (~200 nm) and continuous layer with uniform distribution on the surface (Figure 4). There are no obvious broken chips, as in Figure 3, on the surface, with some minor cracks present. The surface coating layer shows no apparent delamination, most probably due to the nature of the thin surface layer.

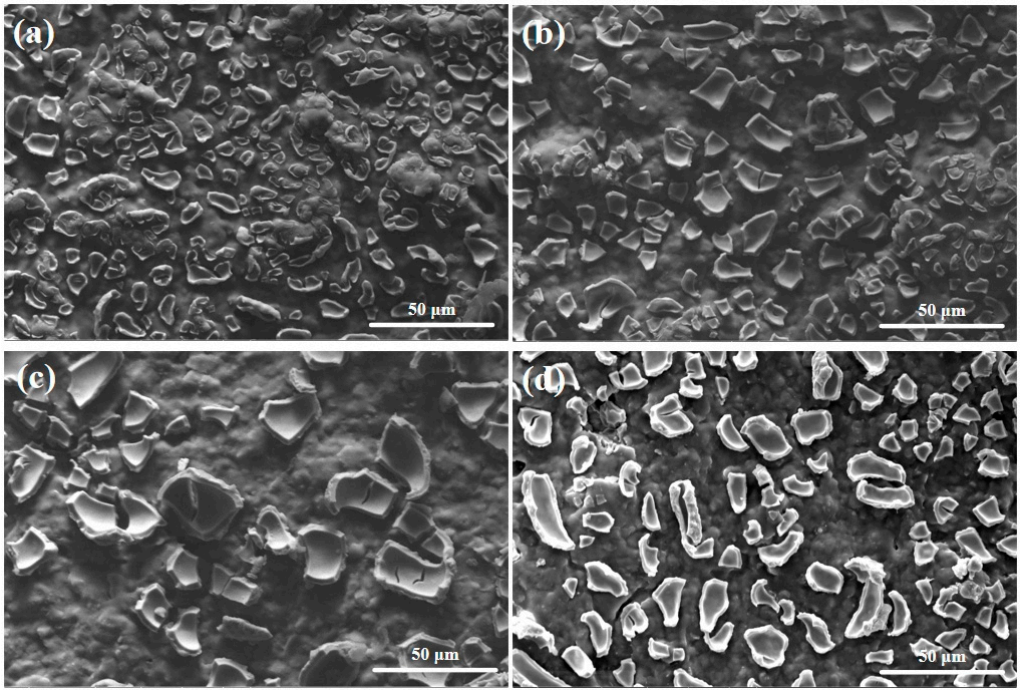


Figure 5. SEM morphologies of the samples dip-coated by four different sols: (**a**) LSZ; (**b**) LBZ; (**c**) HBZ; and (**d**) YSZ on the baked (800 °C) bodies, followed by second sintering (1150 °C).

The surface zirconia layer with sol precursor dipped on the surface of the baked (800 °C) body shows an obviously different morphology (Figure 5) from the others. The zirconia layer remained flaky with less curled chips compared to the one on the green body (Figure 3). The surface zirconia coating is uniformly distributed with almost no cracking on the body underneath. HBZ and LBZ samples showed thicker coatings with larger edge curling. The LSZ coating was thinner (~2 µm), with less curling but contained fragmented particles. All the coated samples on the baked body exhibited distinct "tile-like" micron-scale structures. Based on surface SEM analysis, the coating thickness was estimated to range from approximately 2 µm for the LSZ sample to several micrometers for the HBZ and LBZ samples.

2.3. Phase Analysis of Surface Coatings (XRD)

Figure 6 shows the XRD patterns of samples prepared with YSZ sol dip-coated on three different bodies. Peaks corresponding to Fe_2O_3, mullite, and quartz (body phases) are present in all samples. Distinct ZrO_2 peaks are observed in both green and baked body samples and identified as the monoclinic phase. No distinct ZrO_2 peaks were detected in the samples coated on pre-sintered bodies. No separate Y_2O_3 peaks were observed in any sample group.

2.4. Porosity and Pore Structure (Mercury Porosimetry)

Mercury porosimetry results (Table 1) for a baked coated purple pottery sample showed a porosity of 3.75% and a volume median pore diameter (D_v) of approximately 197,213 nm (~0.2 mm). An uncoated sintered purple pottery sample had a porosity of 1.2% and a D_v of 71.6 nm.

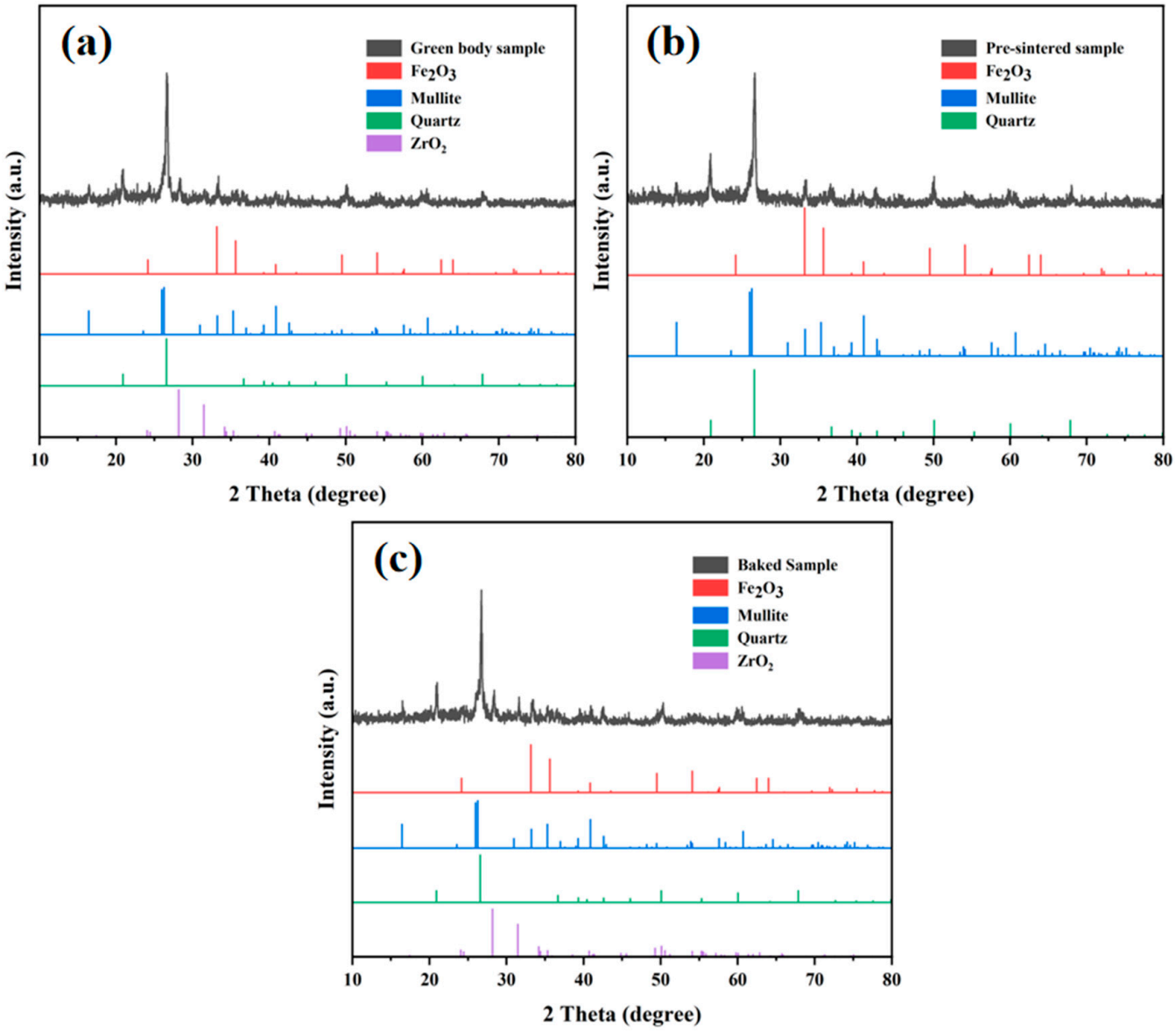


Figure 6. XRD patterns of the YSZ sample coated on a (**a**) green body, (**b**) pre-sintered body, and (**c**) baked body.

Table 1. Porosity and median pore diameter (volume) according to mercury porosimetry.

Sample	Porosity/%	D_v/nm
Sample with baked coatings	3.8	197,212.6
Sample without coatings	1.2	71.6

2.5. Surface Capillary Effect

A comparative test was performed on a baked (800 °C) small Jianshui purple pottery bowl, partially coated with YSZ sol (left side of the white line), followed by general sintering at 1150 °C. An obvious difference in capillary effect for the coated and uncoated area was

observed. A water stain spread over a larger area on the coated surface region compared to the uncoated region (Figure 7).

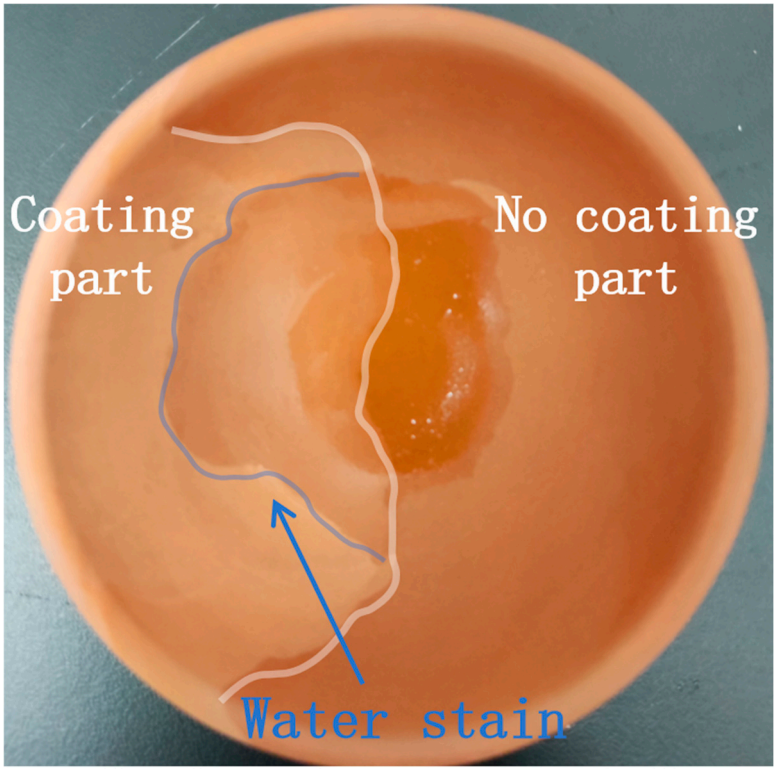


Figure 7. Test of the capillary effect on the surface of a small purple pottery bowl partially coated by ZiO_2. The left side of the white line is the coated area, and the right side is the original purple pottery (uncoated) area. The blue line marks the area where the water stain spread. The area of the water stain on the coated part is significantly larger than that on the uncoated part.

2.6. Antibacterial Performance

Antibacterial tests (*Escherichia coli*, *E. coli*) were compared for coated and uncoated samples (on base bodies) after loading with silver nanoparticles (AgNPs) and undergoing an accelerated desorption treatment (boiling in water for 1 h). Plate counting results (Figure 8, Table 2) showed that the coated sample loaded with AgNPs had an average bacterial concentration of 3.54×10^5 CFU/mL, corresponding to an antibacterial rate of 32.7% compared to the uncoated control sample without AgNPs (5.26×10^5 CFU/mL). The uncoated sample loaded with AgNPs showed a concentration of 4.69×10^5 CFU/mL (antibacterial rate of 10.8%).

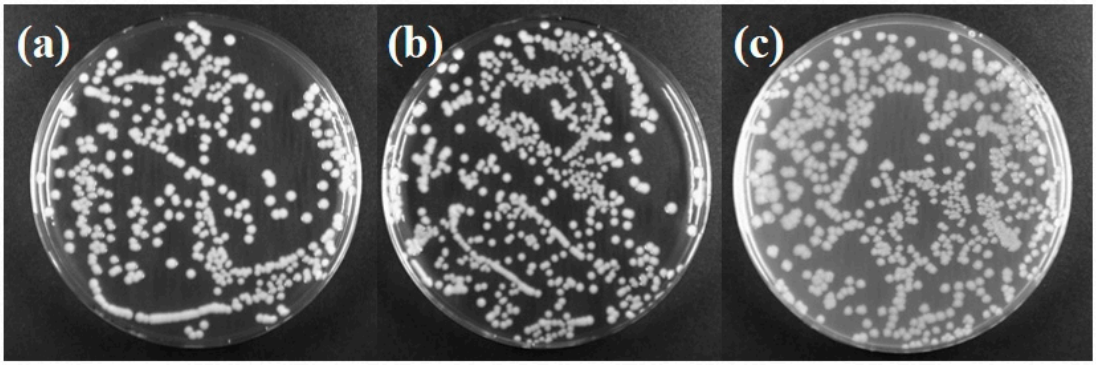


Figure 8. Pictures of flat colony counting: (**a**) coated samples with AgNPs, (**b**) original samples with AgNPs, and (**c**) coated samples without AgNPs.

Table 2. Antibacterial ability test results.

Sample	Average Colony Count	Dilution Factor	Bacterial Suspension Concentration (CFU/mL)	Antibacterial Rate
Baked coated samples loaded with silver nanoparticles	354	10^2	3.54×10^5	32.7%
Uncoated samples loaded with silver nanoparticles	469	10^2	4.69×10^5	10.8%
Pre-sintered coated samples without silver nanoparticles loaded	526	10^2	5.26×10^5	/

3. Discussion

3.1. Mechanism of the Formation of Surface Coating Layer

The main difference in the appearance of the surface coating layer arises from the interplay among shrinkage, porosity, affinity for the sol, and the resulting interfacial stresses of the bodies.

The completely dried body (green body) is highly hydrophilic and porous, allowing for deep penetration of the sol precursor into the surface layer of the body, which promotes the integration of the coating materials and the bodies. During the drying process, most of the water on the sol slowly dried out, and the solid particles coalesced, forming separate chips on the surface. During this process, part of the body's particles might also migrate into the surface sol layer, especially in the case of larger particles, forming a complex surface layer with both pottery particles and zirconia particles, which has a solid bond with the body underneath. During subsequent sintering, both the body and the surface chips underwent substantial shrinkage. Due to the strong interaction between the surface chips and the body, the shrinkage of the surface chips might cause the cracking of the shallow surface of the body, as well as the curling of the surface chips. Since the particle sizes of the surface particles are in nanoscale, the shrinkage ratio should be larger than the micrometer scale of the body particles. This difference in shrinkage between the surface particles and the bodies generates high tensile stress between them, leading to the body surface cracking and the eventual peeling of the surface [13], as shown in Figure 9. The LSZ sol, with its lower concentration and smaller particle size, likely generates lower stress during drying and sintering, explaining the absence of severe cracking.

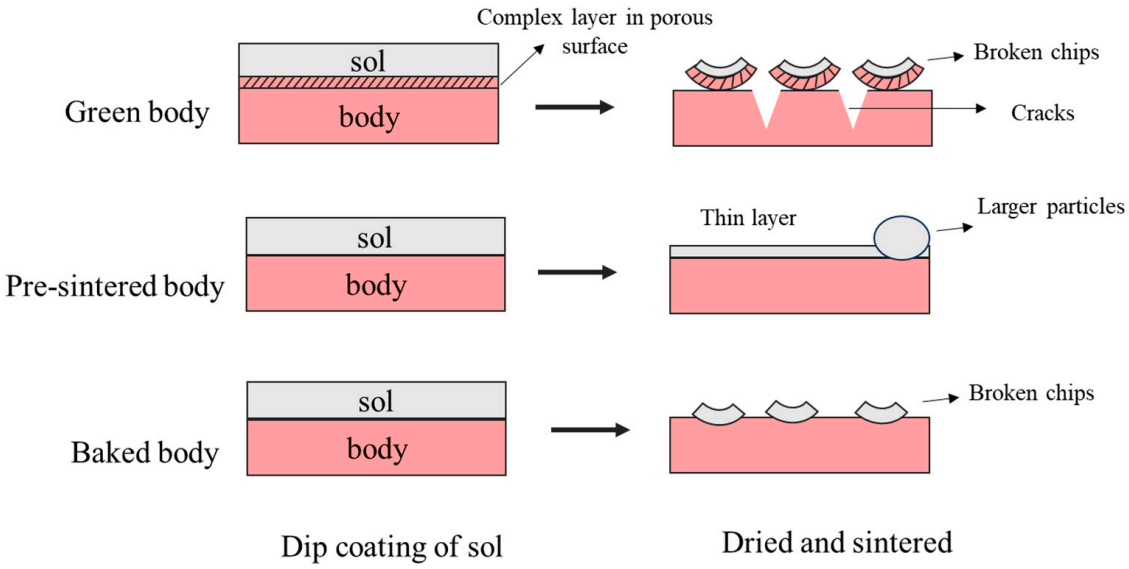


Figure 9. Schematic formation diagram of the surface coating layer.

The pre-sintered body was already fully sintered and densified before application of the ZrO_2 sol. During the drying process, most of the water in the sol precursor was evaporated instead of being sucked into the pores of the body, and most of the particles coalesced and formed large particles, as in the coffee ring effect. That is to say, the surface coating forms thin layers on most surfaces and larger droplets on small areas, forming non-uniform distribution during drying. The resulting coating is thus mostly thin and experiences minimal stress during the second sintering, yielding a continuous, dense, and well-adhered layer. However, this dense structure offers limited specific surface area for further accommodation of secondly functional materials.

The coating on the baked body strikes an optimal balance. Pre-firing at 800 °C allows the bodies to undergo most of the shrinkage [14], reducing the shrinkage mismatch with the coating layer during final sintering. Simultaneously, the baked body retains sufficient porosity and hydrophilicity for the sol to be effectively drawn into surface pores via the capillary effect, ensuring good coating particle embedding and integration with the bodies. The final coating exhibits uniform distribution, strong adhesion, and a unique "tile-like" porous microstructure. This microstructure arises from the cracking of the continuous gel coating during drying and sintering due to residual stress, significantly increasing the specific surface area.

The schematic diagrams of the formation of the morphologies of the coating layer on three different surfaces are shown in Figure 9.

The results also show that the particle concentrations and sizes of the sol significantly affect the coating quality. A high concentration and large particle size (HBZ, LBZ) lead to a thick coating layer, which is more prone to induce severe curling. A lower concentration and smaller particle size (LSZ, YSZ) facilitates the formation of more uniform and stable coatings.

Yttrium doping in the YSZ sol further enhances coating stability. Y^{3+} ions incorporate into the ZrO_2 lattice, as intended by the precursor formulation, stabilizing the monoclinic/tetragonal phases at room temperature and suppressing the destructive monoclinic-tetragonal phase transformation during cooling, which is accompanied by a large volume change [15]. This phase stabilization reduces internal stresses within the coating particles, contributing to better morphological integrity and stronger interfacial bonding between the body and the surface coating layer.

3.2. Enhancement of Surface Properties and Functionality

The mercury porosimetry data confirm that the ZrO_2 coating on the baked body dramatically alters the surface pore structure, shifting the dominant pore size from the nanometer scale (71.6 nm for the body) to the micrometer scale (~200 μm) and increasing the porosity. This created microstructure, along with potential changes in surface wettability, is responsible for the observed enhanced capillary effect (Figure 7).

More importantly, this highly porous, high-surface-area coating serves as an excellent capacitor for immobilizing additional functional nanoparticles, e.g., antibacterial Ag nanoparticles. Although both coated and uncoated surfaces can adsorb Ag NPs, the coated sample retained more AgNPs after the harsh desorption treatment (boiling), leading to superior antibacterial performance (32.7% vs. 10.8% reduction). This is attributed to the physical entrapment of AgNPs within the rough, porous coating structure and potentially stronger interactions with the ZrO_2 surface, making them less susceptible to leaching.

This study demonstrates a practical and effective strategy for functionalizing traditional pottery. The sol–gel coating on the baked body is relatively simple and compatible with existing pottery production. The resulting ZrO_2 coating provides a robust, adherent, and highly porous platform.

While AgNPs were used here as a model functional agent, this platform is versatile. Other functional materials (e.g., antimicrobial agents like ZnO or TiO_2, catalysts, or optical materials) could be loaded. Furthermore, by using template agents or modifying sol–gel parameters, the coating's pore structure and surface chemistry could be finely tuned for specific applications.

This work offers a practical and reproducible approach for the surface modification of traditional pottery. While this study used AgNPs as a model functional agent, the developed ZrO_2 coating platform is versatile and capable of hosting other functional materials (e.g., other antimicrobial agents, catalysts, or optical materials), paving the way for multifunctional pottery while preserving its intrinsic aesthetic.

4. Materials and Methods

4.1. Materials

The purple pottery red clay is produced in Jianshui County, Honghe Hani and Yi Autonomous Prefecture, Yunnan Province, with zirconium (IV) nitrate pentahydrate (99.99%-Zr (REO), Maclin), oxalic acid (99%, Maclin), deionized water, and silver nanoparticle solution (1000 ppm, 10–15 nm (MW), Aladin).

4.2. Characterization

XRD: Rigaku D/max 2610, Cu Kα radiation, and λ = 1.5418 Å; accelerating voltage: 35 kV; tube current: 20 mA; scanning speed: 8°/min; and SEM: QUANTA FEG 250.

4.3. Preparation of Purple Pottery Samples

Raw materials used in the experiment include red clay and white clay for purple pottery produced in Jianshui, Honghe, Yunnan Province, zirconium nitrate pentahydrate (99.99%-Zr (REO)), oxalic acid (99%), and silver nanoparticle solution (1000 ppm, particle size 10–15 nm).

The purple pottery clay is mixed from locally mined "five-color" soils, which are five different types of clay: red soil (also known as patterned soil), white soil, blue soil, yellow soil, and purple soil. The purple pottery red clay is a mixture of these five soils, while the white clay is a mixture of white and blue soils. The main crystalline phases of red, white, blue, and yellow soils are halloysite (a type of aluminosilicate) and quartz. The main crystalline phases of purple soil are andradite and forsterite.

A custom-made polytetrafluoroethylene (PTFE) mold with a square cavity of dimensions 30 mm × 30 mm × 5 mm was used. First, the moisture content of the purple pottery clay was controlled to approximately 25 wt.% through pressing, filtering, and air drying, giving the clay a certain plasticity. A measured amount of clay was pressed into the mold to fill the cavity. After compaction, excess clay was scraped from the surface. The sample was then air dried naturally for two hours. After drying, it was demolded and placed in an electric hot-air-drying oven for at least five hours. After complete drying, the green body dimensions were approximately 29 mm × 29 mm × 5 mm, and after sintering, approximately 27 mm × 27 mm × 4 mm. All purple pottery sample tiles selected for the experiment were those without cracks or significant warping during the drying process.

4.4. Preparation of Metal Oxide Coatings

The samples were prepared by directly dip-coating the purple pottery bodies into the sol, followed by drying and sintering. This method has minimal impact on the original production process and is easier to implement compared to more complex coating methods.

Using zirconium nitrate as the precursor and oxalic acid as a hydrolysis promoter, three different zirconium hydroxide sols were prepared by adjusting the amounts of reactants,

reaction temperature, reaction time, and oxalic acid addition. The hydrolysis reaction of zirconium nitrate is as follows:

$$Zr(NO_3)_4 + 3H_2O \rightarrow ZrO(OH)_2 + 4HNO_3$$

Both reaction temperature and oxalic acid addition accelerate the above reaction, increasing the rate of $ZrO(OH)_2$ colloid particle formation and the driving force for particle growth, thereby increasing particle size. Increasing reaction time leads to more frequent collisions between colloid particles due to thermal motion, also enhancing particle agglomeration [16]. The preparation processes are as follows:

(1) Dissolve 4.293 g of $Zr(NO_3)_4 \cdot 5H_2O$ in 100 mL of deionized water, heat to 60 °C with stirring until completely dissolved. Add 0.280 g of $H_2C_2O_4 \cdot 2H_2O$, then raise the temperature to 90 °C and react for 24 h. Filter after reaction completion. The Zr concentration in the sol is 0.1 mol/L, and dynamic light scattering (DLS) testing showed a volume distribution around 50 nm. This sol has low colloid concentration and small particle size (low concentration and small size), designated as LSZ.

(2) Dissolve 12.879 g of $Zr(NO_3)_4 \cdot 5H_2O$ in 100 mL of deionized water, heat to 60 °C with stirring until completely dissolved. Add 0.420 g of $H_2C_2O_4 \cdot 2H_2O$, then raise the temperature to 90 °C and react for 19 h. Filter after reaction completion. The Zr concentration in the sol is 0.3 mol/L, and DLS testing showed a volume distribution around 100 nm. This sol has high colloid concentration and large particle size (high concentration and big size), designated as HBZ.

(3) Dissolve 4.293 g of $Zr(NO_3)_4 \cdot 5H_2O$ in 100 mL of deionized water, heat to 60 °C with stirring until completely dissolved. Add 0.315 g of $H_2C_2O_4 \cdot 2H_2O$, then raise the temperature to 90 °C and react for 24 h. Filter after reaction completion. The Zr concentration in the sol is 0.1 mol/L, and DLS testing showed a volume distribution around 100 nm. This sol has low colloid concentration and large particle size (low concentration and big size), designated as LBZ.

(4) Dissolve 4.293 g of $Zr(NO_3)_4 \cdot 5H_2O$ and 0.3788 g of $Y(NO_3)_3 \cdot 6H_2O$ in 100 mL of deionized water, heat to 60 °C with stirring until completely dissolved. Add 0.280 g of $H_2C_2O_4 \cdot 2H_2O$, then raise the temperature to 90 °C and react for 24 h. Filter after reaction completion. The Zr concentration in the sol is 0.1 mol/L, and DLS testing showed a volume distribution around 50 nm. This sol has low colloid concentration and small particle size and is an yttria-stabilized zirconia (YSZ) sol, designated as YSZ.

4.5. Sol Coating Methods

The three sols, which should not be stored for over 3 days, were applied to the red clay purple pottery tile substrates using the following different methods.

(1) Green Body Coating: The dried purple pottery red clay green body tiles were directly immersed in the sol for approximately 5 s with a withdrawal speed of ~2 mm/s. After dipping, they were placed in an electric hot-air-drying oven at 60 °C for at least 2 h. After completely drying, they were placed in a muffle furnace and fired according to the firing curve shown in Figure 10.

(2) Pre-sintered Body Coating: The dried purple pottery red clay tiles were placed in a muffle furnace and fired to the sintering temperature according to the sintering schedule in Figure 10a. After sintering, they were immersed in the sol for approximately 5 s with a withdrawal speed of ~2 mm/s. After dipping, they were placed in an electric hot-air-drying oven at 60 °C for at least 2 h. After completely drying, they were placed in a muffle furnace and fired again according to the firing curve shown in Figure 10.

(3) Baked Body Coating: The dried purple pottery red clay tiles were pre-fired to 800 °C, according to the pre-firing curve in Figure 10b, and then naturally cooled to room temperature. They were then immersed in the sol for approximately 5 s with a withdrawal speed of ~2 mm/s. After dipping, they were placed in an electric hot-air-drying oven at 60 °C for at least 2 h. After completely drying, they were placed in a muffle furnace and fired according to the firing curve shown in Figure 10a.

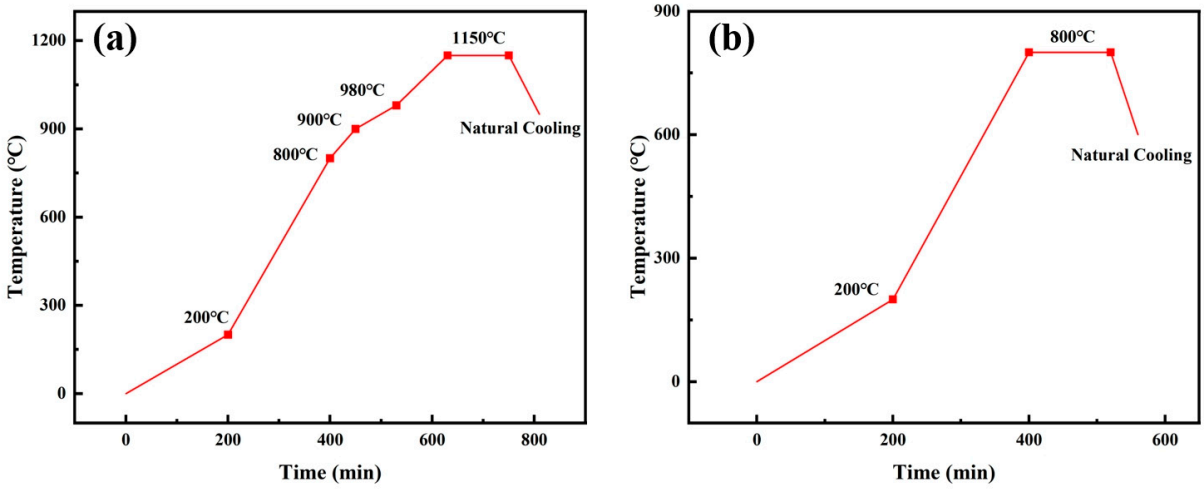


Figure 10. (**a**) Firing curve and (**b**) preheating curve of coating sample.

4.6. Antibacterial Ability Test Methods

The baked coated samples and uncoated samples were pretreated by immersing them in a silver nanoparticle (AgNP) solution for 30 min, followed by drying. Subsequently, they were subjected to boiling in water for 1 h to accelerate the desorption of AgNPs, simulating the conditions of daily use for purple pottery products. The antibacterial capabilities of these two sample types were then assessed using a co-culture method combined with plate counting to evaluate the AgNP loading capacity. A baked coated sample without AgNP loading served as the blank control group.

The specific antibacterial testing procedure was as follows: All samples were sterilized at 121 °C for 15 min prior to testing. *Escherichia coli* (*E. coli*) was used as the bacterial strain. A bacterial culture tube containing 3 mL of nutrient broth liquid medium was inoculated with a single colony picked from a solid bacterial culture plate. The bacterial culture was then incubated overnight in a constant temperature shaker at 37 °C and 200 rpm. The bacterial suspension was adjusted to approximately 10^5 CFU/mL using phosphate-buffered saline (PBS), and 75 mL was added to each conical flask. The samples were placed into the flasks for co-culture with the bacterial suspension. After 24 h of shaken incubation, the bacterial suspension was appropriately diluted, and the colony count was determined using nutrient agar medium. Figure 10 shows images of the colonies from plate counting.

5. Conclusions

This work analyzed and explored coating materials and strategies suitable for purple potteries. Four different sols were prepared and applied onto pottery bodies treated with three different methods (green body, pre-sintered body, and baked body). The coated samples based on baked bodies achieved better performances than the others. The coating effects are also related to particle concentrations and sizes of the sol. A high concentration and large particle size lead to increased coating thickness, greater curling of the zirconia coating edges, and poorer coating-body bonding strength. Among all the prepared sols, the YSZ sol exhibited the best coating effect. Doping with Y_2O_3 further stabilizes

the ZrO_2 crystalline phase, effectively reducing the impact of volume changes caused by phase transformation during sintering, allowing zirconia particles to better maintain their morphology. Coated samples showed a better loading capacity for AgNP compared to the uncoated samples. The sol–gel-derived ZrO_2 coating on baked Jianshui purple pottery exhibits uniform morphology, strong adhesion, and a porous structure suitable for functional nanoparticle loading. The demonstrated antibacterial (*Escherichia coli*) performance (32.7% reduction) highlights its potential for functional pottery applications. The coated samples are more compatible with functional metal particles compared to the original purple potteries, enabling purple potteries to possess novel functions for wider application scenarios.

Author Contributions: Conceptualization, Z.G., J.L., P.Z. and A.S.; Methodology, J.H.; Validation, J.L. and Q.N.; Formal analysis, Z.G.; Investigation, Z.G., J.H. and Q.N.; Resources, Y.B. and Z.H.; Writing—original draft, Z.G. and J.H.; Writing—review & editing, P.Z.; Supervision, P.Z.; Project administration, L.G.; Funding acquisition, Y.H. All authors have read and agreed to the published version of the manuscript.

Funding: This research was funded by Yunnan Provincial Science and Technology Talent & Platform Program grant number [202305AF150051] and Scientific and Technological Project of Yunnan Precious Metals Laboratory (YPML-20240502002).

Institutional Review Board Statement: Not applicable.

Informed Consent Statement: Not applicable.

Data Availability Statement: The original contributions presented in this study are included in the article. Further inquiries can be directed to the corresponding author..

Conflicts of Interest: Authors Yu He, Yuan Bao and Zixuan He were employed by the company Jianshui Chongwen Tongchuang Purple Clay Culture Co., Ltd. The remaining authors declare that the research was conducted in the absence of any commercial or financial relationships that could be construed as a potential conflict of interest.

References

1. Kishitake, K.; Era, H.; Otsubo, F.; Sonoda, T. Improvement of the adhesion of a ceramic coating on a ceramic substrate. *Therm. Spray. Tech.* **1998**, *7*, 64–70. [CrossRef]
2. Holländer, A.; Cosemans, P. Surface technology for additive manufacturing. *Plasma Process. Polym.* **2020**, *17*, 1900155. [CrossRef]
3. Wei, Q.; Wang, D.; Zhang, S. Research Progress on Surface Modification Technology of Inorganic Ceramic Membranes. *J. Funct. Mater.* **1999**, 601–603.
4. Zhang, J.; Song, K.; Zhang, M.; Zhao, Z.; He, Q.; Li, Z. Development Trends of High-Performance Ceramic Coatings and Their Preparation Processes. *Surf. Technol.* **2017**, *46*, 96–103.
5. Abdelrahman, M.M. Study of Plasma and Ion Beam Sputtering Processes. *J. Phys. Sci. Appl.* **2015**, *5*, 128–142. [CrossRef]
6. Hou, L.; Wang, H.; Zeng, L. Traditional Surface Modification Techniques of Ceramic Materials. *Shandong Ceram.* **2004**, 21–25.
7. Zhang, J.; Hou, Y.; Gao, L.; Li, F. Research on Surface Modification of Nanoscale SiC Powder by Non-uniform Nucleation Coating Method. *J. Silic. Sci.* **1998**, *26*, 762–767.
8. Yin, Z.; Wang, S.; Fu, W.; Tan, X.; Tao, S.; Ding , C. Evolution and Prospect of Thermal Spraying Technology. *J. Inorg. Mater.* **2011**, *26*, 225–232. [CrossRef]
9. Huang, C.; Yin, S.; Li, W.; Guo, X. Research Status and Prospects of Cold Spraying Technology and Its System. *Surf. Technol.* **2021**, *50*, 1–23.
10. Brinker, C.J.; Frye, G.C.; Hurd, A.J.; Hurd, A.J.; Ashley, C.S. Fundamentals of Sol-gel Dip Coating. *Thin Solid. Film.* **1991**, *201*, 97–108. [CrossRef]
11. Meng, Y. Technology of Nano Thin Aluminum Oxide Composite Micro-Diboride Titanium Conductive Coating. Kunming University of Science and Technology, Kunming, China, 2004.
12. Liu, Y.W.; Nong, Z.S. Research Status of Ceramic Coatings Prepared by Sol-Gel Method. *Cailiao Baohu* **2023**, *56*, 173–179.
13. Birnie, D.P.; Kaz, D.M.; Taylor, D.J. Surface Tension Evolution During Early Stages of Drying of Sol-gel Coatings. *J. Sol-Gel Sci. Technol.* **2009**, *49*, 233–237. [CrossRef]

14. He, J.; Wang, Y.; Gan, Z.; He, Y.; Zhang, P.; Liu, J.; Na, Q.; Shan, A.; Gao, L. A Brief Analysis of the Composition and Firing Issues of Jianshui Purple Clay. *Jiangsu Ceram.* **2024**, *57*, 43–50.
15. Feinberg, A.; Perry, C.H. Structural Disorder and Phase Transitions in ZrO_2-Y_2O_3 System. *J. Phys. Chem. Solids* **1981**, *42*, 513–518. [CrossRef]
16. Southon, P.D.; Bartlett, J.R.; Woolfrey, J.L.; Ben-Nissan, B. Formation and Characterization of an Aqueous Zirconium Hydroxide colloid. *Chem. Mater.* **2002**, *14*, 4313–4319. [CrossRef]

Disclaimer/Publisher's Note: The statements, opinions and data contained in all publications are solely those of the individual author(s) and contributor(s) and not of MDPI and/or the editor(s). MDPI and/or the editor(s) disclaim responsibility for any injury to people or property resulting from any ideas, methods, instructions or products referred to in the content.